ELSEVIER

Journal of Biomechanics 37 (2004) 1899–1911

JOURNAL OF BIOMECHANICS

www.elsevier.com/locate/jbiomech
www.JBiomech.com

Numerical investigation of the non-Newtonian blood flow in a bifurcation model with a non-planar branch

Jie Chen, Xi-Yun Lu*

Department of Modern Mechanics, University of Science and Technology of China, Hefei, Anhui 230026, PR China

Accepted 23 February 2004

Abstract

The non-Newtonian fluid flow in a bifurcation model with a non-planar daughter branch is investigated by using finite element method to solve the three-dimensional Navier–Stokes equations coupled with a non-Newtonian constitutive model, in which the shear thinning behavior of the blood fluid is incorporated by the Carreau–Yasuda model. The objective of this study is to investigate the influence of the non-Newtonian property of fluid as well as of curvature and out-of-plane geometry in the non-planar daughter vessel on wall shear stress (WSS) and flow phenomena. In the non-planar daughter vessel, the flows are typified by the skewing of the velocity profile towards the outer wall, creating a relatively low WSS at the inner wall. In the downstream of the bifurcation, the velocity profiles are shifted towards the flow divider. The low WSS is found at the inner walls of the curvature and the lateral walls of the bifurcation. Secondary flow patterns that swirl fluid from the inner wall of curvature to the outer wall in the middle of the vessel are also well documented for the curved and bifurcating vessels. The numerical results for the non-Newtonian fluid and the Newtonian fluid with original Reynolds number and the corresponding rescaled Reynolds number are presented. Significant difference between the non-Newtonian flow and the Newtonian flow is revealed; however, reasonable agreement between the non-Newtonian flow and the rescaled Newtonian flow is found. Results of this study support the view that the non-planarity of blood vessels and the non-Newtonian properties of blood are an important factor in hemodynamics and may play a significant role in vascular biology and pathophysiology.

Keywords: Non-Newtonian fluid flow; Non-planar artery; Carotid bifurcation; Hemodynamics

1. Introduction

Atherosclerosis, a localized disease, often occurs at the carotid bifurcation, the coronary bifurcation, the infra-renal aorta and so on. The localization of the atherosclerosis in the artery may be due to local variations in wall shear stress (Delfino et al., 1997). There are three risk factors for the development of the atherogenesis (Araim et al., 2001; Wang et al., 2002), which include low shear stress region, high vessel pressure distribution, and high particle residence time in the region of the atherosclerosis. It is well known that specific sites in the arterial tree are sensitive to the formation of the atherosclerotic lesions. Local hemodynamics is believed to play an important role in the development of these lesions in the sinus of the carotid bifurcation (Caro et al., 1971; Friedman et al., 1981; Zarins et al., 1983; Nerem, 1992). In fact, local hemodynamics are not only governed by the geometry of the bifurcation and the properties of the arterial wall, but also by the rheological properties of blood. On the other hand, the non-planarity of the artery is also an important factor influencing arterial flows and the curvature of the aortic arch is approximately helical (Caro et al., 1996).

Recently, researchers have performed a lot of work on blood flow in order to disclose the reason of the atherogenesis theoretically (e.g., Sarkar and Jayraman, 1998) and experimentally (e.g., Zhao et al., 2000; Ding et al., 2001). However, the theoretical analysis was limited to deal with some simple problem, while the experiment was time-consuming and costly. The numerical simulations have been developed to become an important tool in the investigation of the blood flow in

*Corresponding author. Tel.: +86-551-3603223; fax: +86-551-3606459.
E-mail address: xlu@ustc.edu.cn (X.-Y. Lu).

0021-9290/$ - see front matter © 2004 Elsevier Ltd. All rights reserved.
doi:10.1016/j.jbiomech.2004.02.030

the artery. Some work has been performed using the computational fluid dynamics methods, including the non-Newtonian blood flow (Lou and Yang, 1993), the unsteady blood flow (Tu and Deville, 1996), the three-dimensional complex geometries (Hofer et al., 1996; Santamarina et al.,1998; Weydahl and Moore, 2001; Lee et al., 2001; Lu et al., 2002), multi-branch (Shipkowitz et al.,1998) and even reconstructed from the realistic artery with the data from the experiment (Friedman and Ding, 1998; Perktold et al., 1998). But the conditions mentioned above are considered apart and the synthetic influence of the conditions has not been well analyzed. Some researchers have paid their attention on the influence of the non-Newtonian properties of blood on the flow in three-dimensional bifurcation model (Gijsen et al., 1999a, b). Recently, the present authors (Lu et al., 2002, Wang et al., 2002) have numerically investigated the influence of the non-planarity artery with bifurcation on the flow and wall shear stress. However, to the authors' knowledge, little work has been performed to incorporate the non-Newtonian fluid properties in the equations of motion to investigate the flow and wall shear stress in the non-planarity artery with bifurcation.

In this study, the feature of the non-Newtonian properties of fluid on the velocity distribution and wall shear stress in a non-planarity artery with bifurcation is investigated. The three-dimensional Navier–Stokes equations coupled with the non-Newtonian constitutive model are numerically solved by a finite element method. To compare the flow behavior of the non-Newtonian fluid with that of the Newtonian fluid, calculated results for the Newtonian fluid with original Reynolds number and the corresponding rescaled Reynolds number are given. Based on our calculated results, the synthetic influence of the non-planarity of the blood vessel and the non-Newtonian properties of the blood on the flow through three-dimensional artery bifurcation are discussed and analyzed.

2. Methods

The flow is assumed to be steady and laminar. The governing equations are the three-dimensional incompressible Navier–Stokes equations and are given as

$$\rho\left(\frac{\partial \mathbf{u}}{\partial t}+\mathbf{u}\cdot\nabla\mathbf{u}\right)=-\nabla p+\nabla\cdot\mathbf{T}, \tag{1}$$

where u is the fluid velocity vector, ρ the density and p the pressure. T is the stress tensor and linearly dependent on the rate of deformation tensor D with a relation of $\mathbf{T}=2\eta(\dot\gamma)\mathbf{D}$, where $D=\frac{1}{2}(\nabla\mathbf{u}+\nabla\mathbf{u}^{\mathrm{T}})$, η represents the viscosity of the blood, and $\dot\gamma$ is the shear rate. For a non-Newtonian fluid, η is a function of $\dot\gamma$, while for a Newtonian fluid η is a constant and independent of the shear rate $\dot\gamma$. The divergence-free condition is imposed on the velocity u

$$\nabla\cdot\mathbf{u}=0 \tag{2}$$

Here, we consider the blood as a non-Newtonian fluid. As well known, the shear thinning and viscoelasticity of blood (Chien et al., 1970; Thurston, 1973, 1979) are closely relevant to its microscopic structures, e.g., aggregation, deformation and alignment of the red blood cells, where the red blood cells determine mainly the rheological behavior of blood. Investigation on non-Newtonian steady flow in a carotid bifurcation model indicates that the shear thinning is the dominant non-Newtonian property of the blood and the viscoelasticity may be ignored for the prediction of the velocity distribution (Gijsen et al., 1999a, b), even though the importance of the viscoelasticity of the blood analog fluids on the flow phenomena has been presented by Liepsch and Moravec (1984), Ku and Liepsch (1986). In this study, the shear thinning is accounted for by using the Carreau–Yasuda model (Bird et al., 1987) for the viscosity,

$$\frac{\eta-\eta_\infty}{\eta_0-\eta}=[1+(\lambda\dot\gamma)^a]^{(n-1)/a}, \tag{3}$$

where $\dot\gamma$ represents a scalar quantity of the rate of deformation tensor, defined as $\dot\gamma=\sqrt{2tr(D^2)}$ and $D=[\nabla\mathbf{u}+(\nabla\mathbf{u})^{\mathrm{T}}]/2$. The other parameters in Eq. (3) are employed from the experimental data based on the analog blood fluid (Gijsen et al., 1999a, b) and written as $\eta_\infty=2.2\times10^{-3}$ Pa s, $\eta_0=22\times10^{-3}$ Pa s, $\lambda=0.110$ s, $a=0.644$, $n=0.392$ and $\rho=1410\,\mathrm{kg\,m^{-3}}$.

To compare the behavior between the non-Newtonian and Newtonian fluid flows, the corresponding Newtonian fluid, which was used by Gijsen et al. (1999a, b) in their experimental and computational study, is also calculated here. Based on the experimental data of the analog blood fluid (Gijsen et al., 1999a, b), a concentrated solution of potassium thiocyanate in water (KSCN, 71% by weight) was employed as the Newtonian control fluid with the initial Newtonian viscosity $\eta=2.9\times10^{-3}$ Pa s. Then, the original Reynolds number for the Newtonian fluid flow can be obtained as 270 based on the diameter of the mother tube, the mean velocity in the inlet and the fluid density (Gijsen et al., 1999a).

Further, to define a rescaled Reynolds number, a characteristic shear rate (i.e., $\dot\gamma_c$) is needed. The characteristic shear rate for the blood flow in larger arteries can be defined in various ways. Some definitions are employed based on wall shear rate (e.g. Mann and Tarbell, 1990; Cho and Kensey, 1991), which in fact is often the highest shear rate occurring in blood flow, while others are by use of the shear rate based on an average value (e.g. Baaijens et al., 1993; Ballyk et al., 1994; Thurston, 1979). Here, as used by Gijsen et al.

(1999b), Thurston (1973, 1979) and Baaijens et al. (1993), a definition of the characteristic shear rate is given as

$$\dot{\gamma}_c = \frac{2V}{a}, \tag{4}$$

where V and a represent the mean velocity at the inlet of mother tube and the radius of the mother tube. Using the above mentioned parameters in the experiment of Gijsen et al. (1999a, b), the rescaled Reynolds number is calculated as 92.2 approximately, which is about three times lower than the Reynolds number for the Newtonian fluid flow.

Fig. 1 shows a hypothetical three-dimensional non-planar artery with bifurcation that was used in our previous work (Lu et al., 2002). The configuration model is demonstrated from three directions in Figs. 1(b)–(d), respectively. In this model, the mother vessel and the daughter vessels have the same diameter (D). The mother vessel has a length of $3D$. The bifurcation is symmetric and planar and the bifurcating angle is 90°. One daughter vessel is straight with a length of $8D$, and the other one is straight planar $1.5D$ along the axial and then undergoes 45° bending with a radius of $4D$ before it straightens up for a further length of $4D$.

Following the previous study (Weydahl et al., 2001; Lu et al., 2002), at the initial time, the velocity in the whole field is assumed to be zero. At the inlet, a fully developed velocity profile is imposed. The vessels are assumed rigid, and the velocity conditions obey the no-slip and no-penetration constraints on the walls. At the exit of each daughter vessel, a constant pressure and a zero axial velocity gradient are used.

A finite element method based on the fractional-step velocity correction (Kovacs and Kawahara, 1991; Lu et al., 2002) is used to numerically solve Eqs. (1) and (2).

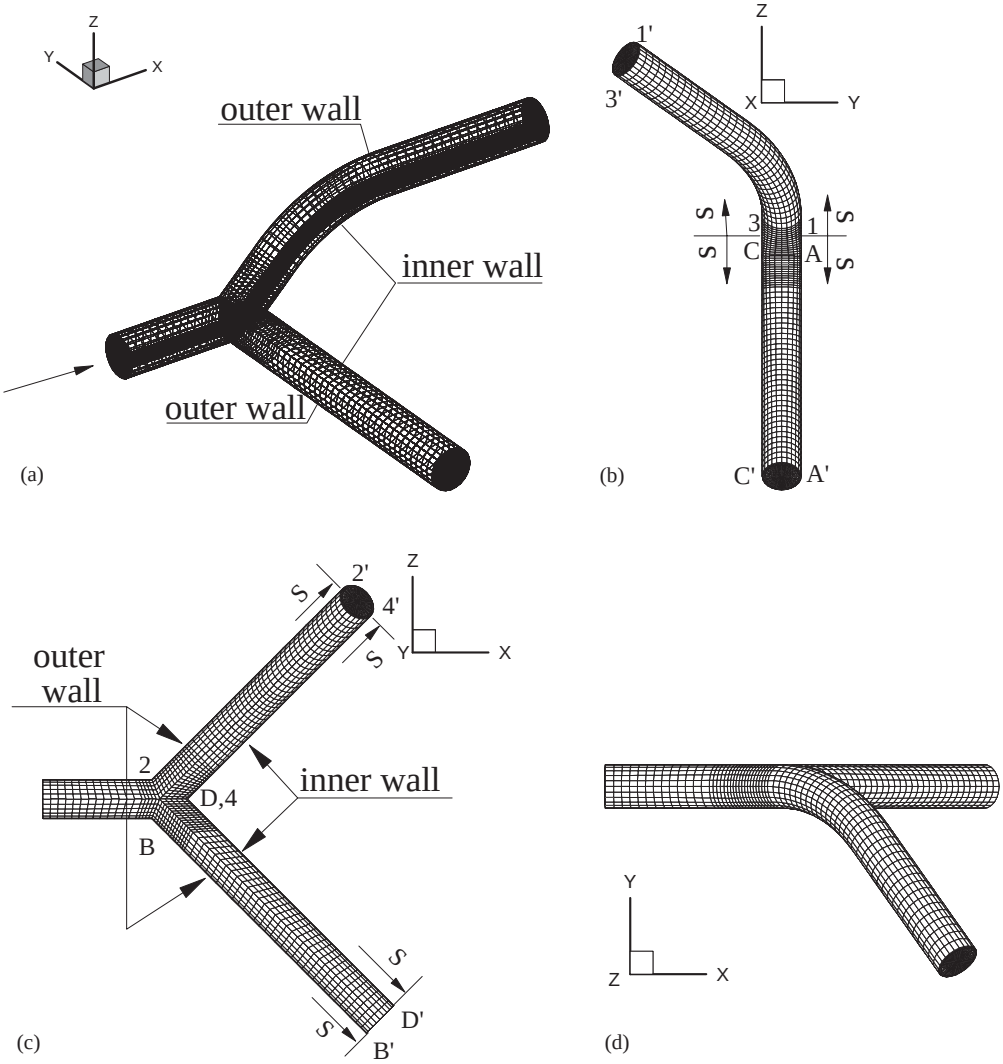

Fig. 1. Geometry of three-dimensional bifurcation model with a non-planar daughter branch: (a) global view; (b) view face to x-direction; (c) view from y-direction; (d) view face to z-direction.

The finite element spatial discretization is performed using the Galerkin—weighted residual method. The discretized formulation was described by Kovacs and Kawahara (1991) in detail.

3. Results

To validate the present calculation, a typical case of unsteady non-Newtonian entry flow in a 90° curved tube, which was investigated experimentally and numerically by Gijsen et al. (1999b), is used. Based on the flow pulse given by Gijsen et al. (1999b), Fig. 2 shows the axial velocity profiles at end diastole in the plane of symmetry and perpendicular this plane for the non-Newtonian fluid mentioned in Eq. (3) for the viscosity. The corresponding experimental and numerical results obtained by Gijsen et al. (1999b) are also plotted in Fig. 2. It is found that the present results are in quite good agreement with those previous data. Meanwhile, the axial velocity profiles both at begin diastole and at peak systole agree well the experimental and numerical data (Gijsen et al., 1999b) too. Further, the present computational code has also been verified in our previous study (Lu et al., 2002). Thus, it can be confirmed that our calculation is reliable for the prediction of the flow behavior and wall shear stress (WSS) in the non-planar artery with bifurcation.

Numerical analysis is carried out on the non-Newtonian fluid flow and on the Newtonian fluid flow with the original Reynolds number and the rescaled Reynolds number in a bifurcation model with a non-planar daughter branch, as shown in Fig. 1 for the sketch. The axial velocity profiles, secondary motion and WSS distribution in the non-planar and planar daughter vessels are obtained and analyzed.

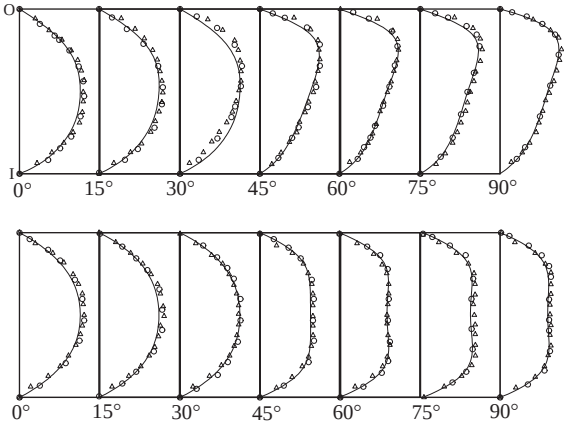

Fig. 2. Axial velocity profiles at end diastole in the plane of symmetry (top) and perpendicular this plane (bottom) for the non-Newtonian fluid and the comparison with the experimental and numerical results (Gijsen et al., 1999b). Here symbols △ and ○ denote the experimental and numerical data given by Gijsen et al. (1999b), and solid line means the present result.

Fig. 3 shows the development of the axial velocity along the non-planar daughter vessel in the bifurcation plane. Flow separation on the outer wall of the vessel near the entry section of the non-planar daughter vessel is identified from the velocity profile at $S = 0.5$, where the distance S is normalized by the mother vessel diameter. Then, the velocity profiles are shifted toward the flow-dividing wall (i.e., the inner wall of the bifurcation). In the region where the non-planar-bending tube switches to the straight tube, the velocity profiles are slightly skewed toward the outer wall again at $S = 5$ approximately. Then the velocity profile approaches asymptotically to be symmetric when the effects of curvature and bifurcation are negligible. By comparing the velocity profiles of the Newtonian flow with those of the non-Newtonian flow, the axial velocity distributions of the non-Newtonian flow show significant flattening and are skewed to the inner wall. It is seen that the velocity profiles of the non-Newtonian flow agree well with those of the rescaled Newtonian fluid flow though somewhat differences appear for the maximum value of the axial velocity distribution. These behaviors are well consistent with the results obtained experimentally and computationally by Gijsen et al. (1999a, b).

The profiles of the axial velocity along the planar daughter vessel in the bifurcation plane are shown in Fig. 4. The flow separation on the outer wall of the vessel near the entry section of the planar daughter vessel is formed at $S = 0.5$. In the downstream of the bifurcation, the velocity profiles are shifted toward the inner wall and show significant flattening for the non-Newtonian fluid. Meanwhile, the profiles of the rescaled Newtonian fluid are also consistent with these of the non-Newtonian fluid. By comparing the velocity profiles along the non-planar vessel in Fig. 3 with those along the planar vessel in Fig. 4, curvature variation caused by bifurcation from the mother tube motivates flow skews to the inner wall. After branch curves out of symmetrical plane, another kind of curvature variation is caused, the superposition of the two types of curvature effects results in flow to deviate some from the divider wall to non-divider wall in the non-planar branch, as shown in Fig. 3 for $S = 5$ and 6.

The axial velocity profiles in the bending plane are shown along the non-planar vessel in Fig. 5 and along the planar vessel in Fig. 6, respectively. Typical M-shape velocity profiles are formed and are consistent with observation in abdominal aorta model and coronary artery branch by Perktold et al. (1998). In Fig. 5, it is seen that the velocity profiles are skewed towards the outer wall (i.e., generating line 1–1′ in Fig. 1) of the curved vessel along the non-planar vessel from $S = 2.5$ approximately. However, the velocity profiles are

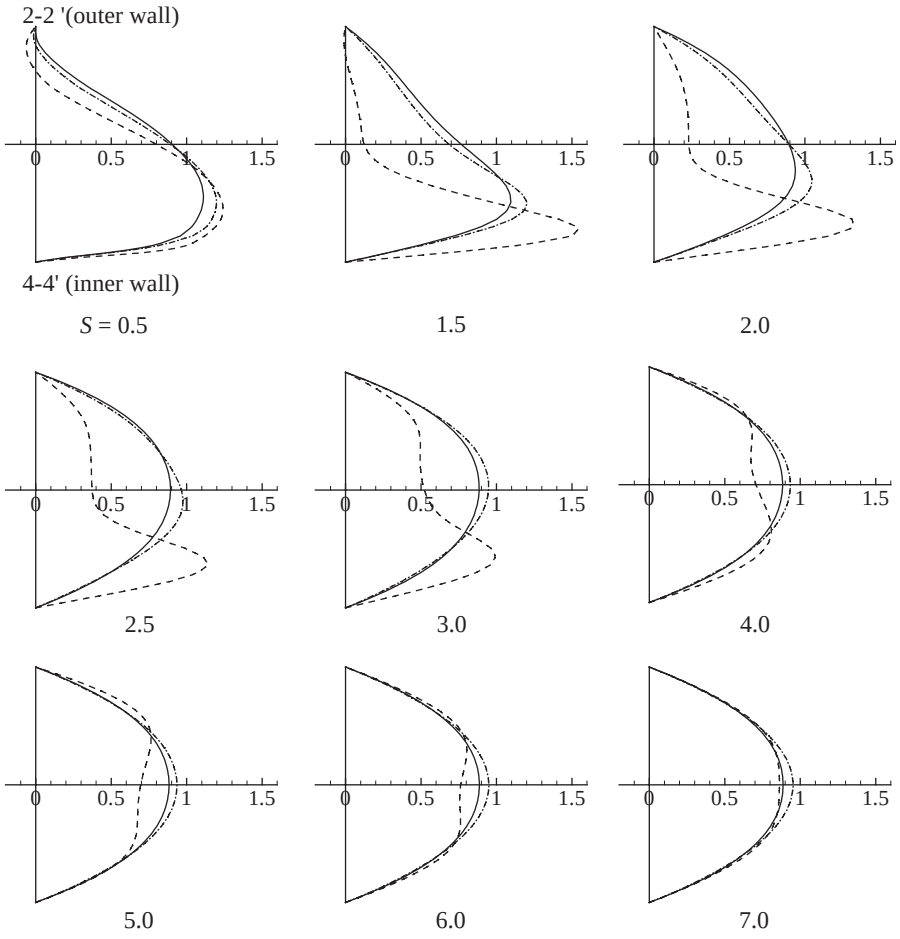

Fig. 3. Axial velocity profiles at several cross-sections along the non-planar daughter vessel in the bifurcation plane (2–2′ and 4–4′ shown in Fig. 1) for non-Newtonian (solid line), Newtonian (dashed line), and rescaled Newtonian fluid flow (dash–dot line).

symmetric along the planar vessel in Fig. 6. Based on our calculated results, it can be evidently seen that the difference between the velocity distributions of the non-Newtonian and Newtonian fluids is reasonably predicted. Because of the shear-thinning behavior of the non-Newtonian fluid, the velocity field is flattened, and has lower velocity gradients at the inner walls and positive velocity gradients at the outer walls. The typical M-shape velocity profiles become less evident. As expected, the profiles of the axial velocity between the non-Newtonian and the rescaled Newtonian fluids agree well each other along the planar and non-planar daughter vessels in Figs. 5 and 6.

The axial velocity contours at several cross-sections along the non-planar and planar daughter vessels for the non-Newtonian and Newtonian fluid are shown in Fig. 7. The swirling effect is better illustrated in the axial velocity contours at those sections. The crescent contours of the axial velocity change from skewed to the inner wall near the bifurcation to a more parabolic profile with flow through along the vessel. In the bend, flow deviates from the inner wall of the bifurcation to its sidewall. Due to the curvature of the non-planar vessel, the crescent shape rotates along the vessel in the anti-clockwise direction viewing from the end of the daughter vessel, which agrees with results by Sherwin et al. (2000). However, the crescent shape rotation along the vessel is very weak for the non-Newtonian fluid, and axisymmetrical pattern is gradually formed along the vessel. Those contours are consistent with the axial velocity profiles in Figs. 3–6, where the flattening velocity profiles are reasonably predicted due to the shear-thinning behavior of the non-Newtonian fluid. The corresponding contours of the rescaled Newtonian fluid (not shown here) are also examined, as expected, are consistent with the patterns of the non-Newtonian fluid.

Secondary flow streamlines at different sections along the non-planar and planar vessels for the non-Newtonian fluid flow are shown in Fig. 8. There are pronounced movement of fluid from the outer wall of the bifurcation towards the inner wall, caused by the pressure gradient induced by the curvature in the vessel. At sections close to the bifurcation, counter-rotating vortices (Dean vortices) are evident. The secondary

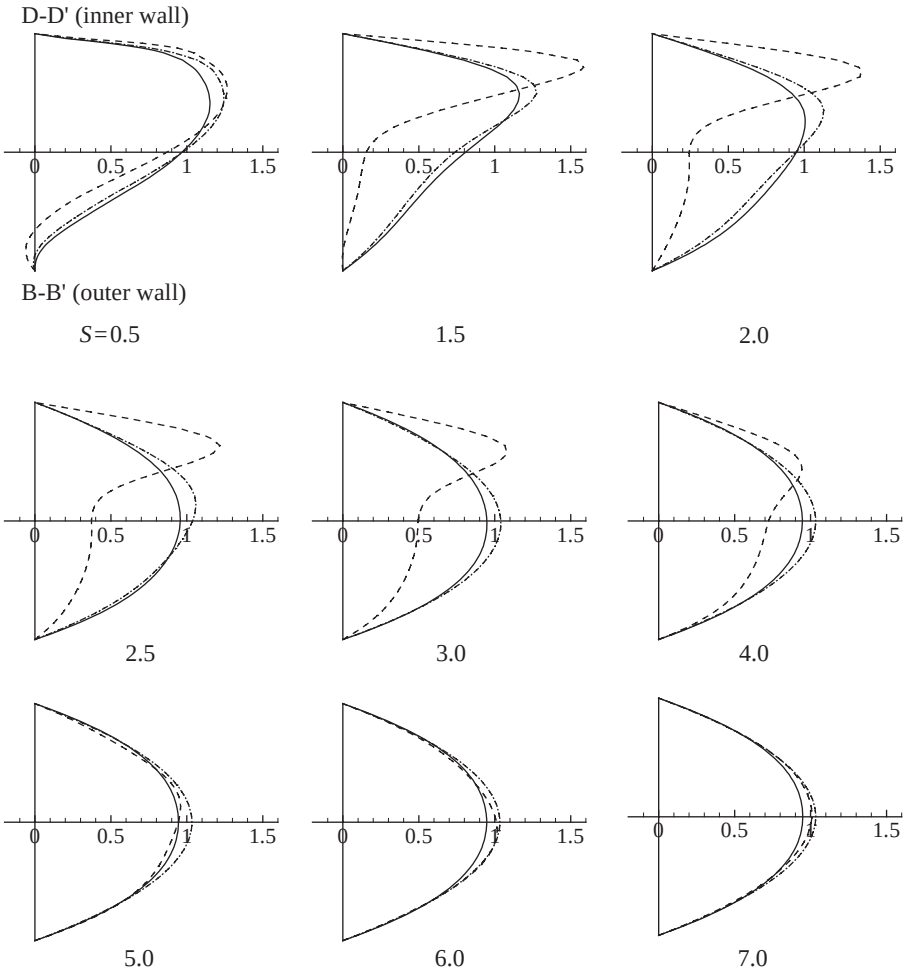

Fig. 4. Axial velocity profiles at several cross-sections along the planar daughter vessel in the bifurcation plane (B–B′ and D–D′ shown in Fig. 1) for non-Newtonian (solid line), Newtonian (dashed line) and rescaled Newtonian fluid flow (dash–dot line).

flows weaken in strength along the vessel. In the planar vessel, the streamlines are nearly symmetric and there are two counter rotating vortices. In the non-planar vessel, the two vortices are asymmetric, which reflects the influence of the curvature due to the out-of-plane bend.

To illustrate WSS behavior, the distributions of WSS along four generating lines on the non-planar and planar daughter vessels are shown in Figs. 9 and 10, respectively. Those results demonstrate that there exists significant difference of WSS between the non-Newtonian and Newtonian flows due to the shear-thinning effect of the non-Newtonian fluid. Such the behavior of the distribution of WSS for the non-Newtonian and Newtonian flows is well consistent with the data obtained experimentally and computationally by Gijsen et al. (1999a, b). Illustrations in Figs. 9 and 10 compare the magnitude of WSS between the non-planar and planar vessels at the inner and the outer walls of the bifurcation plane as well as those of the bending plane. It is found that peak WSS exists on the inner wall in the bifurcation plane near the entry section of the daughter vessel in Figs. 9(d) and 10(d). The profiles of WSS predicted by the non-Newtonian and Newtonian flows agree well each other for $S<1.5$ and exhibit significant difference between them for $S<1.5$ It is noted to see that the profile of WSS calculated by the rescaled Newtonian fluid depicts a higher peak than those by the non-Newtonian and Newtonian fluids at $S=0.3$ approximately, and agrees well with that by the non-Newtonian fluid for $S<1.5$ On the outer wall of the bifurcation plane in Figs. 9(b) and 10(b), the WSS is nearly close to zero at $S<1.5$ approximately for the non-Newtonian flow and the rescaled Newtonian flow and at $S<1.5$ for the Newtonian flow. The distribution of WSS of the non-Newtonian flow is higher than that of the Newtonian flow for $S<1.5$ approximately. This behavior agrees with the analysis and prediction of the vascular biology and pathophysiology (Araim et al., 2001).

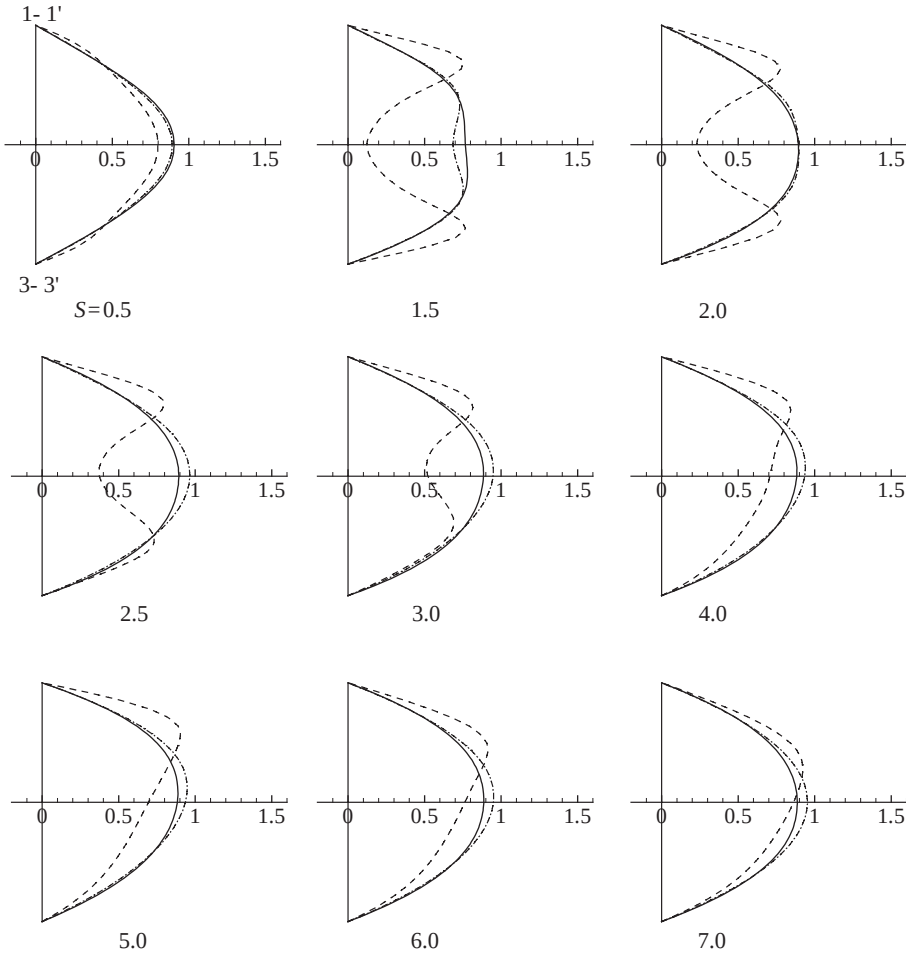

Fig. 5. Axial velocity profiles at several cross-sections along the non-planar daughter vessel in the bending plane (1–1′ and 3–3′ shown in Fig. 1) for non-Newtonian (solid line), Newtonian (dashed line) and rescaled Newtonian fluid flow (dash–dot line).

As shown in Figs. 9(a), (d), 10(a) and (c), the out-of-plane bend results change in WSS, but the most significant change occurs in the bending plane. At the inner wall of the bend in Figs. 9(c) and 10(c), the WSS over the section of the bend is reduced on an average by 10–15% compared to that in the planar vessel. The WSS of the non-Newtonian flow is higher than that of the Newtonian flow over the inner wall of the bend. However, at the outer wall of the bend in Figs. 9(a) and 10(a), the opposite behavior occurs, and the WSS over the section of the bend is increased on average by 10–15% compared to that in the planar vessel due to the non-planarity effect. The WSS of the non-Newtonian flow is higher than that of the Newtonian flow over the section of the non-planar daughter vessel. These findings agree well with the changes in flow distributions caused by the out-of-planar bend and correspond to the rotation of the axial flow in the curved branch, and are qualitatively consistent with the experimental data and calculated results (Gijsen et al., 1999a, b).

Compared to the profiles of WSS of the non-Newtonian flow in Figs. 9 and 10, the rescaled Newtonian fluid model underestimates wall shear stresses in low wall shear rate regions and overestimates wall shear stresses in high shear rate regions. Actually, as indicated by Gijsen et al. (1999a, b), application of the rescaled Newtonian fluid is hard to be generalized to all geometries and flow conditions. Basically, as shown in Figs. 9 and 10, the WSS of the rescaled Newtonian flow is reasonably consistent with the data of the non-Newtonian flow along both the inner and the outer walls of the bifurcation plane as well as along both the inner and the outer walls of the bend.

4. Discussion and conclusion

As well known, the WSS is the tangential force caused by the flow of blood along the surface of the endothelium. It has been believed that the atherosclerotic plaques form in the regions of low WSS and disturbed flow. Using both in vivo and in vitro models, it has been demonstrated that vessels, which are prone to plaque formation, have the flow patterns character-

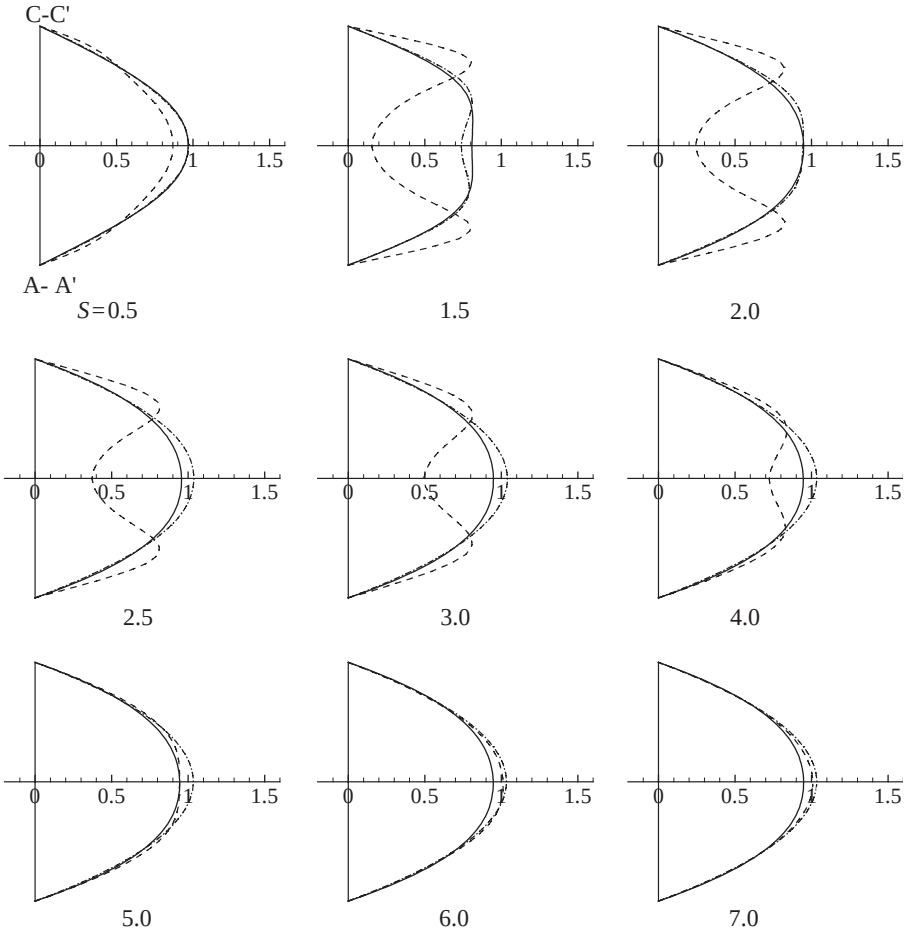

Fig. 6. Axial velocity profiles at several cross-sections along the planar daughter vessel in the bending plane (A–A′ and C–C′ shown in Fig. 1) for non-Newtonian (solid line), Newtonian (dashed line) and rescaled Newtonian fluid flow (dash–dot line).

ized by low WSS, flow separation and stasis, and oscillations of flow (Araim et al., 2001). The appearance of low WSS appears to coincide with early intimal thickening in the carotid artery (Ku et al., 1985) and abdominal aorta (Moore et al., 1994). As described for the calculated results shown in the above, the velocity is skewed toward the flow divider and the low WSS is found at the inner walls of curvature and the lateral walls of bifurcations. Fluid flow in curved vessels is typified by the skewing of the velocity profile towards the outer wall, creating a relatively low WSS at the inner wall. These behaviors are consistent with the previous findings (Caro et al., 1978; Pedley, 1980). Generally, the configuration and branch angle of the internal carotid sinus produce an area of low WSS and alter hemodynamics along the outer wall of the vessel, where atherosclerotic plaques tend to be formed.

The non-planarity of artery has an important influence on arterial flows and the curvature of the aortic arch is approximately helical (Caro et al., 1996). As shown in Fig. 8, secondary flow patterns that swirl fluid from the inner wall of curvature to the outer wall in the middle of the vessel have been well documented for curved and bifurcating vessels. Considering the fully developed flow field in a helically symmetric tube, the secondary flow changes from a single vortex to a pair of symmetrical vortices (Dean flow) as the Dean number increases, and the shear stress reduces by increasing the non-planarity of the helical tube. These results agree well with the observations predicted by Zabielski and Mestel (1998a, b) and support the hypothesis of Kamiya and Togawa (1980) that arteries adapt their shape in order to reduce excessive WSS.

Usually, local hemodynamic behaviors depend not only on the geometry of the bifurcation and the properties of the arterial wall, but also on the rheological properties of blood. Difference between the velocity distributions for the Newtonian and non-Newtonian fluid is evident. In the common carotid artery the non-Newtonian fluid shows a flattened axial velocity profile due to its shear thinning behavior. In the internal carotid artery, the non-Newtonian velocity field is flattened, and has lower velocity gradients at the divider wall and positive velocity gradients at the

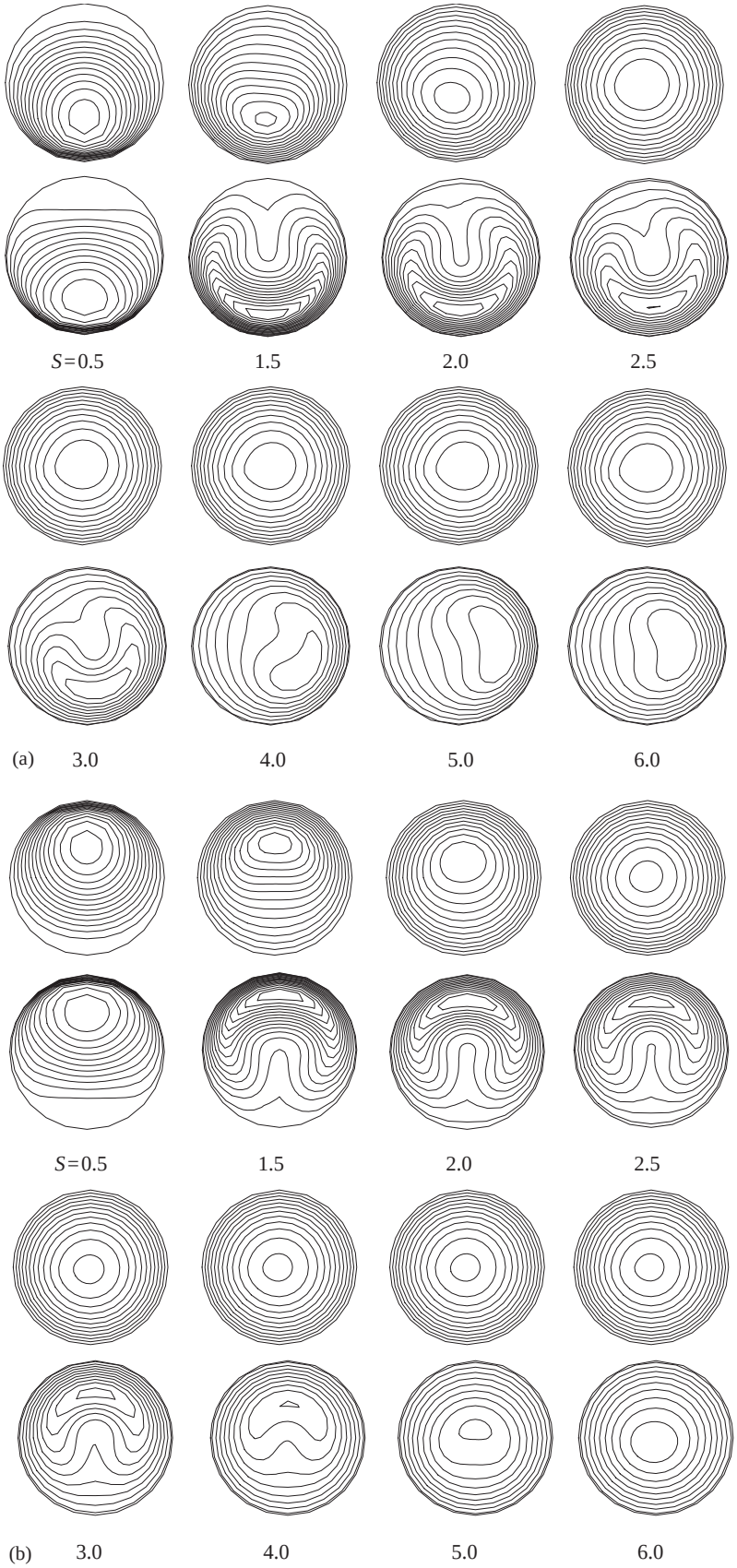

Fig. 7. Contours of the axial velocity component in several cross-sections for non-Newtonian (top) and the Newtonian fluid (bottom): (a) along the non-planar daughter vessel; (b) along the planar daughter vessel.

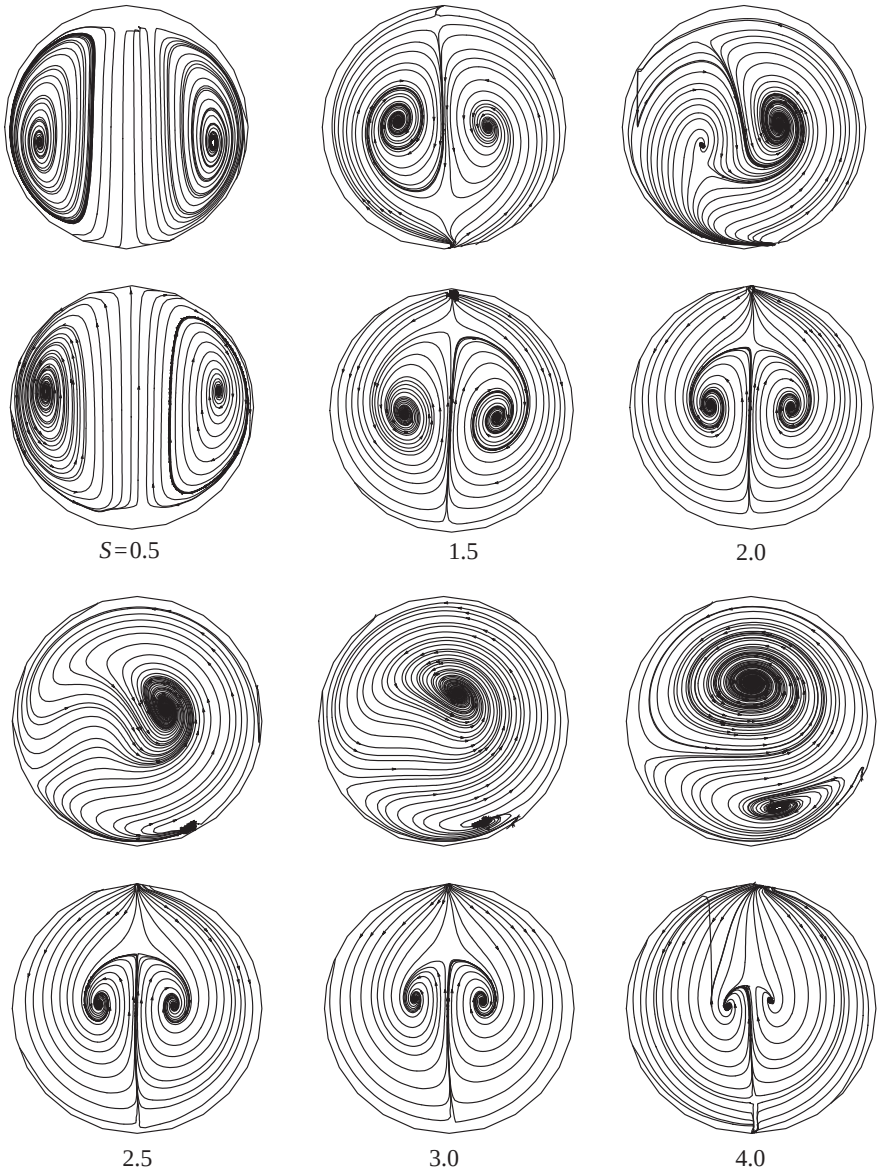

Fig. 8. Secondray flow streamlines for non-Newtonian fluid in several cross-sections along the non-planar daughter vessel (top) and along the planar daughter vessel (bottom).

non-divider wall. Furthermore, the curvature-induced secondary flow seems to be less dominant for the non-Newtonian fluid. Meanwhile, based on previous experimental and numerical work (Gijsen et al., 1999a, b), the shear thinning property is the dominant non-Newtonian property of the blood analog fluid and viscoelasticity may be ignored for the prediction of the velocity distribution. The effect of the non-Newtonian properties including only the shear thinning behavior on the velocity distribution and WSS in the planar and non-planar daughter vessels is exhibited in this study.

The shear thinning behavior of the blood allows for approximation by a viscosity evaluated at the characteristic shear rate of the flow. The results, including the flow field and WSS in the daughter vessels, of the scaled Newtonian flow compare well to these of the non-Newtonian flow. Usually, the definition of the characteristic shear rate is under dispute. Following the present calculated results, the agreement between the non-Newtonian and rescaled Newtonian velocity field indicates that a definition of the characteristic shear rate, based on an average shear rate, as proposed by Thurston (1979), Baaijens et al. (1993) and Gijsen et al. (1999a, b), is appropriated. As shown in the above, the value of the Reynolds number for the rescaled Newtonian flow, based on the characteristic viscosity, is about one third of the Reynolds number for the initial Newtonian flow. Furthermore, as indicated by Gijsen

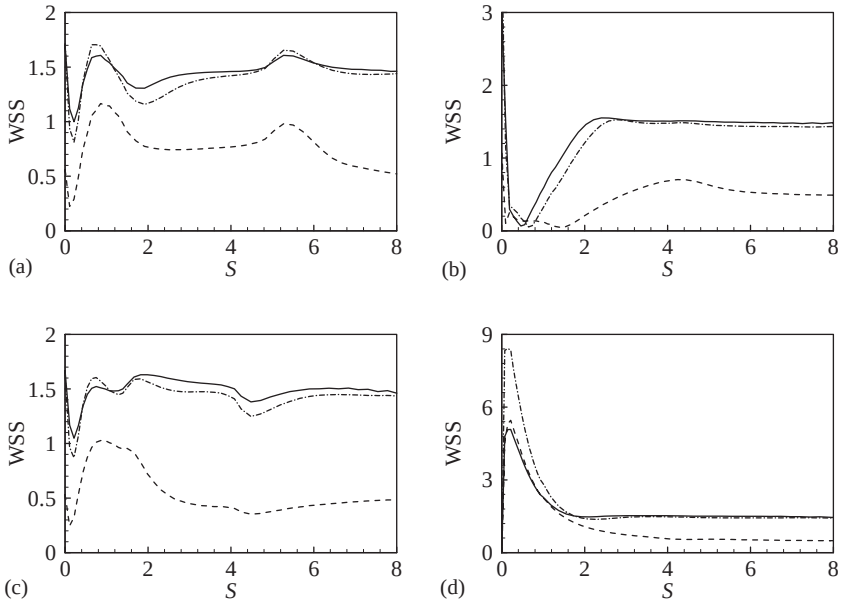

Fig. 9. Distributions of WSS along four generating lines on the non-planar daughter vessel for non-Newtonian (solid line), Newtonian (dashed line) and rescaled Newtonian fluid flow (dash–dot line): (a) 1–1′; (b) 2–2′; (c) 3–3′; (d) 4–4′.

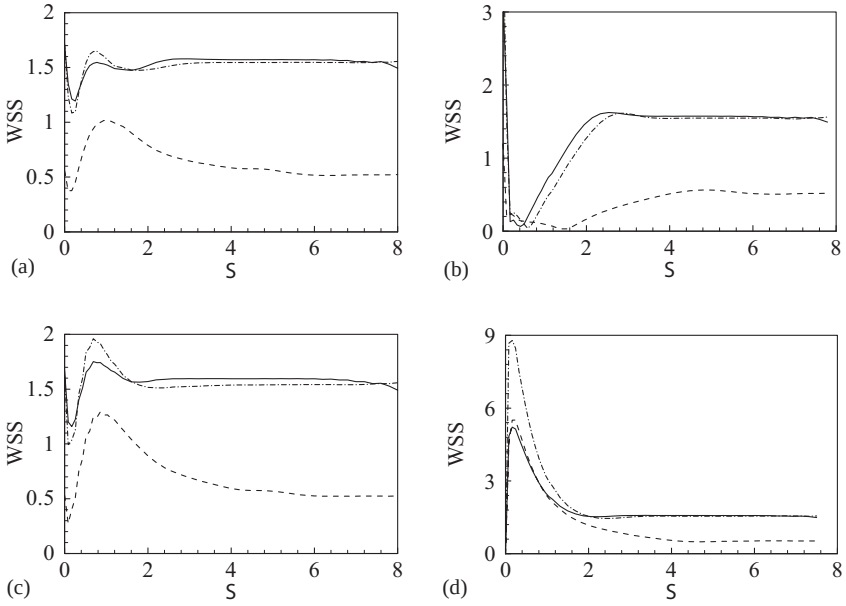

Fig. 10. Distributions of WSS along four generating lines on the planar daughter vessel for non-Newtonian (solid line), Newtonian (dashed line) and rescaled Newtonian fluid flow (dash–dot line): (a) A–A′; (b) B–B′; (c) C–C′; (d) D–D′.

et al. (1999a, b), the sensitivity to the characteristic shear rate could also help to explain the difference between the flow fields in younger and older individuals (Reneman et al., 1985). As the characteristic shear rate in the older individuals is lower, the characteristic viscosity is higher. Thus, the absence of flow reversal in the internal carotid artery in the older individuals could be explained. However, the characteristic shear rate is higher for younger individuals, and blood is therefore expected to behave more like a Newtonian fluid flow.

Based on the calculated results described in the above, concluding remarks are briefly summarized as follows. The influence of the non-Newtonian properties of blood and the non-planarity of the daughter branch on WSS, velocity distribution and flow field in the non-planar and planar daughter vessels is analyzed. In the curvature pipe of the non-planar daughter vessel, the flow is typified by the skewing of the velocity profile toward the outer wall, creating a relatively low-WSS on the inner wall. In the bifurcation vessel, the velocity is shifted

toward the flow divider. The low WSS distributions are found at the inner walls of the curvature and the lateral walls of the bifurcation. The non-Newtonian fluid shows a flattened axial velocity profile due to its shear thinning behavior and has lower velocity gradients at the divider wall and positive velocity gradients at the non-divider wall. Secondary flow patterns that swirl fluid from the inner wall of curvature to the outer wall in the middle of the vessel are also well documented for the curved and bifurcating vessels. However, the curvature-induced secondary flow seems to be less dominant for the non-Newtonian fluid. The appearance of the low WSS appears to coincide with early intimal thickening in the carotid artery and abdominal aorta. All those findings of this study suggest that the non-Newtonian properties of blood and the non-planarity in blood vessels are important in hemodynamic effect. They affect the interaction between flows and the vessel and are likely to alter residence time of particles and biological cells in the close vicinity of the vascular endothelium, and may thus play an important role in vascular biology and pathophysiology.

Acknowledgements

The authors are in debt to Professors W. Wang and L.-X. Zhuang for their helpful comments and discussion. This work was supported by the National Natural Science Foundation (No. 10028205), the Outstanding Overseas Chinese Scholars Fund of Chinese Academy of Sciences, and the Hundred-Talent Programme of Chinese Academy of Sciences.

References

Araim, O., Chen, A.H., Sumpio, B., 2001. Hemodynamic forces: effects on atherosclerosis. New Surgery 1, 92–100.

Baaijens, J.P.W., van Steenhoven, A.A., Janssen, J.D., 1993. Numerical analysis of steady generalized newtonian flow in a 2D model of the carotid artery bifurcation. Biorheology 30, 63–74.

Ballyk, P.D., Steinman, D.A., Ethier, C.R., 1994. Simulation of non-newtonian blood flow in an end-to-side anastomosis. Biorheology 31, 565–586.

Bird, R.B., Armstrong, R.C., Hassager, O., 1987. Dynamics of Polymer Liquids, Vol. 1, 2nd edition. Wiley, New York.

Caro, C.G., Pedley, T.J., Schroter, R.C., Seed, W.A., 1978. The Mechanics of the Circulation. Oxford University Press, Oxford.

Caro, C.G., Doorly, D.J., Tarnawski, M., Scott, K.T., Long, Q., Dumoulin, C.L., 1996. Non-planar curvature and branching of arteries and non-planar-type flow. Proceedings of the Royal Society of London B 452, 185–197.

Caro, C.G., Baker, A.J., Fitzgerald, J.M., Schroter, R.C., 1971. Atheroma and arterial wall shear: observations, correlation and proposal of a shear dependent mass transfer mechanism for atherogenesis. Proceedings of the Royal Society of London B 117, 109–159.

Chien, S., Usami, S., Dellenback, R.J., Gregersen, M.I., 1970. Sheardependent deformation of erythrocytes in rheology of human blood. American Journal of Physiology 219, 136–142.

Cho, Y.I., Kensey, R., 1991. Effects of the non-newtonian viscosity of blood flows in a diseased arterial vessel. Part 1: steady flows. Biorheology 28, 241–262.

Delfino, A., Stergiopulos, N., Moore Jr, J.E., Meister, J.J., 1997. Residual strain effects on the field in a thick wall finite element model of the human carotid bifurcation. Journal of Biomechanics 30, 777–786.

Ding, Z.R., Wang, K.Q., Li, J., Cong, X.S., 2001. Flow field and oscillatory shear stress in a tuning-fork-shaped model of the average human carotid bifurcation. Journal of Biomechanics 34, 1555–1562.

Friedman, M.H., Ding, Z.H., 1998. Variability of the planarity of the human aortic bifurcation. Medical Engineering and Physics 20, 469–472.

Friedman, M.H., Peters, O.J., Bargero, C.B., Hutchins, G.M., Mark, F.F., 1981. Correlation between intimal thickness and fluid shear in human arteries. Atherosclerosis 39, 425–436.

Gijsen, F.J.H., van de Vosse, F.N., Janssen, J.D., 1999a. The influence of the non-newtonian properties of blood on the flow in large arteries: steady flow in a carotid bifurcation model. Journal of Biomechanics 32, 601–608.

Gijsen, F.J.H., van de Vosse, F.N., Janssen, J.D., 1999b. The influence of the non-Newtonian properties of blood on the flow in large arteries: unsteady flow in a 90° curved tube. Journal of Biomechanics 32, 705–713.

Hofer, M., Rappitsch, G., Perktold, K., Turbel, W., Schima, H., 1996. Numerical study of wall mechanics and fluid dynamics in end-to-side anastomoses and correlation to intimal hyperplasia. Journal of Biomechanics 29, 1297–1308.

Kamiya, A., Togawa, T., 1980. Adaptive regulation of wall shear stress to flow change in the canine artery. American Journal of Physiology 239, H14–H21.

Kovacs, A., Kawahara, M., 1991. A finite element scheme based on the velocity correction method for the solution of the time-dependent incompressible Navier–Stokes equations. International Journal for Numerical Methods in Fluids 13, 403–423.

Ku, D.N., Giddens, D.P., Zarins, C.K., Glagov, S., 1985. Pulsatile flow and atherosclerosis in the human carotid bifurcation: positive correlation between plaque location and low and oscillating shear stress. Atherosclerosis 5 (3), 293–302.

Ku, D.N., Liepsch, D., 1986. The effect of non-newtonian viscoelasticity and wall elasticity on flow at a 90° bifurcation. Biorheology 23, 359–370.

Lee, D., Su, J.M., Liang, H.Y., 2001. A numerical simulation of steady flow fields in a bypass tube. Journal of Biomechanics 34, 1407–1416.

Liepsch, D., Moravec, S., 1984. Pulsatile flow of non-newtonian fluid in distensible models of human arteries. Biorheology 21, 571–586.

Lou, Z., Yang, W.J., 1993. A computer simulation of the non-newtonian blood flow at the aortic bifurcation. Journal of Biomechanics 26, 37–49.

Lu, Y.L., Lu, X.Y., Zhuang, L.X., Wang, W., 2002. Breaking symmetry in non-planar bifurcation: distribution of flow and wall shear stress. Biorheology 39, 431–436.

Mann, D.E., Tarbell, J.M., 1990. Flow of non-newtonian blood analog fluids in rigid curved and straight artery models. Biorheology 27, 711–733.

Moore Jr, J.E., Xu, C., Glagov, S., Zarins, C.K., Ku, D.N., 1994. Fluid wall shear stress measurements in a model of the human abdominal aorta: oscillatory behavior and the relationship to atherosclerosis. Atherosclerosis 110, 225–240.

Nerem, R.M., 1992. Vascular fluid mechanics, the arterial wall, and atherosclerosis. Journal of Biomechanical Engineering 114, 274–282.

Pedley, T.J., 1980. The Fluid Mechanics of Large Blood Vessels. Cambridge University Press, Cambridge.

Perktold, K., Hofer, M., Rappitsch, G., Loew, M., Kuban, B.D., Friedman, M.H., 1998. Validated computation of physiologic flow in a realistic coronary artery branch. Journal of Biomechanics 31, 217–228.

Reneman, R.S., van Merode, T., Hick, P., Hoeks, A.P.G., 1985. Flow velocity patterns in and distensibility of the carotid artery bulb in subjects of various ages. Circulation 71 (3), 500–509.

Santamarina, A., Weydahl, E., Siegel Jr, J.M., Moore Jr, J.E., 1998. Computational analysis of flow in a curved tube model of the coronary arteries: effects of time-varying curvature. Annals of Biomedical Engineering 26, 944–954.

Sarkar, A., Jayaraman, G., 1998. Correction to flow rate—pressure drop relation in coronary angioplasty: steady streaming effect. Journal of Biomechanics 31, 781–791.

Sherwin, S.J., Shah, O., Doorly, D.J., Peiro, J., Papaharilou, Y., Watkins, N., Caro, C.G., Dumoulin, C.L., 2000. The influence of out-of-plane geometry on the flow within a distal end-to-side anastomosis. Journal of Biomechanical Engineering 122, 86–95.

Shipkowitz, T., Rodgers, V.G.J., Franzin, L.J., Chandran, K.B., 1998. Numerical study on the effect of steady axial flow development in the human aorta on local shear stresses in abdominal. Journal of Biomechanics 31, 995–1007.

Thurston, G.B., 1973. Frequency and shear rate dependence of viscoelasticity of human blood. Biorheology 10, 375–381.

Thurston, G.B., 1979. Rheological parameters for the viscosity, viscoelasticity and thixotropy of blood. Biorheology 16, 149–162.

Tu, C., Deville, M., 1996. Pulsatile flow of non-newtonian fluids through arterial stenoses. Journal of Biomechanics 29, 899–908.

Wang, W., Lu, Y.L., Lu, X.Y., Parker, K.H., Zhuang, L.X., 2002. Cross-flow associated with shear stress gradients on the flow-endothelium interaction. 4th World Congress of Biomechanics, Calgary, Canada.

Weydahl, E.S., Moore Jr, J.E., 2001. Dynamic curvature strongly affects wall shear rates in a coronary artery bifurcation model. Journal of Biomechanics 34, 1189–1196.

Zabielsky, L., Mestel, J., 1998a. Steady flow in a helically symmetric pipe. Journal of Fluid Mechanics 370, 297–320.

Zabielsky, L., Mestel, J., 1998b. Unsteady blood flow in a helically symmetric pipe. Journal of Fluid Mechanics 370, 321–345.

Zarins, C.K., Giddens, D.P., Bharadvaj, B.K., Sottiurai, V., Mabon, R.F., Glagov, S., 1983. Carotid bifurcation atherosclerosis: quantitative correlation of plaque localization with flow velocity profiles and wall shear stress. Circulation Research 53, 502–514.

Zhao, S.Z., Xu, X.Y., Hughes, A.D., Thom, S.A., Stanton, A.V., Ariff, B., Long, Q., 2000. Blood flow and vessel mechanics in a physiologically realistic model of a human carotid arterial bifurcation. Journal of Biomechanics 33, 975–984.